AEROELASTIC ANALYSIS AND OPTIMIZATION OF HIGH ASPECT RATIO AND STRUT-BRACED WINGS

Yoann Le Lamer, Joseph Morlier, Emmanuel Bénard, Ping He

AeroBest 2023
Lisboa, 19-21 July 2023

AEROELASTIC ANALYSIS OF HIGH ASPECT RATIO AND STRUT-BRACED WINGS

Yoann Le Lamer[1*], Joseph Morlier[2], Emmanuel Benard[1] and Ping He[3]

1: ISAE-SUPAERO, Université de Toulouse
10 Avenue Édouard Belin, 31400, Toulouse, France
yoann.le-lamer,emmanuel.benard@isae-supaero.fr, http://www.isae-supaero.fr

2: ISAE-SUPAERO, Université de Toulouse, ICA, MINES ALBI, UPS, INSA, CNRS
10 Avenue Édouard Belin, 31400, Toulouse, France
joseph.morlier@isae-supaero.fr, http://www.isae-supaero.fr

3: Department of Aerospace Engineering, Iowa State University
537 Bissell Road, Ames, IA 50011, United States of America
phe@iastate.edu, http://www.aere.iastate.edu

Abstract. *High Aspect Ratio (HAR) and Strut-Braced Wings (SBW) configurations represent promising avenues of research for meeting the challenge of reducing aviation carbon emissions. Both high and low fidelity models have already been developed for the above-mentioned configurations as well as for the NASA Common Research Model (CRM) that will serve as a baseline for performance comparisons. These aero-structural models are then implemented within an in-house aeroelastic framework for analysis and optimization. High-fidelity models correspond to a RANS aerodynamic analysis associated to a 3D wingbox finite-elements (FE) analysis. Conversely, low-fidelity models resort to a VLM aerodynamic analysis associated to a 1D beam model FE analysis. The objective of this work is to use the so developed models to perform multidisciplinary optimization in order to assess performance improvements potential at preliminary design stage. Different levels of fidelity were developed with a multifidelity approach in mind for further developments. The use of a multifidelity approach makes it possible to reduce computational costs by mainly resorting to low-fidelity computations and only running high-fidelity computations when necessary. Then, aeroelastic optimization is carried out on a modified version of the CRM wing with a higher aspect ratio to study aerodynamic gains. Afterwards, a SBW configuration, here the PADRI geometry, is examined to evaluate its mass reduction potential in addition to the drag reduction provided by the increased aspect ratio. This work currently focuses on aeroelastic optimization using a single fidelity, but is to be further extended to a multifidelity approach.*

Keywords: High Aspect Ratio (HAR) wings, Strut-Braced wings (SBW), Aeroelasticity, Multidisciplinary Design Analysis and Optimization (MDAO)

1 INTRODUCTION

Reducing aviation carbon emissions could potentially be achieved through the use of High Aspect Ratio (HAR) [1] and Strut-Braced Wings (SBW) configurations. Multidisciplinary design optimization (MDO), and in particular aerostructural optimization is necessary in order to make the most of these configurations [2]. Preliminary design studies need to be performed in order to evaluate the performance of a large number of aircraft configurations. Specific models has to be developed to this purpose to mitigate initially high computational costs [3].

The issue of computational costs [3] is critical when it comes to aerostructural studies. This can be dealt with by resorting to surrogate models to approximate a system [4], be it for CFD or finite-elements analysis (FEA), using a certain number of samples.

Multifidelity can also be a promising strategy to reduce computational costs. Indeed, when choosing such a method, surrogate models are trained using models with different levels of fidelity, and thus accuracy and computational costs. An algorithm helps find a balance between computation time and physical accuracy.

In this work we use an aeroelastic analysis and optimization framework developed by [5], the aerostructure package [6], which is implemented within the OpenMDAO framework [7].

The final goal of this study is to use aerostructural models of both high and low fidelity to apply a multifidelity approach in order to assess the performance of several configurations of interest in an efficient way. This paper will present the use of high and low fidelity aeroelastic models for the optimization of different configurations. High and low fidelity aeroelastic optimizations are then performed and results compared.

2 TARGETED CONFIGURATIONS

The objective of this work is to study different configurations to assess potential performance improvements through optimization.

The first goal is to study the effects of increasing wing aspect ratio. To this purpose we chose to focus on the uCRM-13.5 model developed in [8]. This model corresponds to a modified version of the NASA CRM model, with an aspect ratio increased by 50%. Main geometrical dimensions are summarized in table 1. Also, uCRM-9.0 geometry will be used as a baseline in order to assess the benefits of increasing the aspect ratio, particularly in term of induced drag reduction. This model corresponds to the undeformed version of NASA Common Research Model (CRM) [9]. The so developed models have been validated using data provided in [8], for both uCRM-9.0 and uCRM-13.5 (see previous paper). Figure 1 presents the geometry of the NASA CRM wing.

The second goal is to study the effects of adding a strut to a high aspect ratio wing, particularly in terms of potential mass reduction. To this purpose we are focusing on the PADRI configuration. Main geometrical dimensions are summarized in table 1. The strut-wing junction is positioned at 42% of half-span and at 50% of the corresponding chord. Figure 2 presents the geometry of the PADRI configuration.

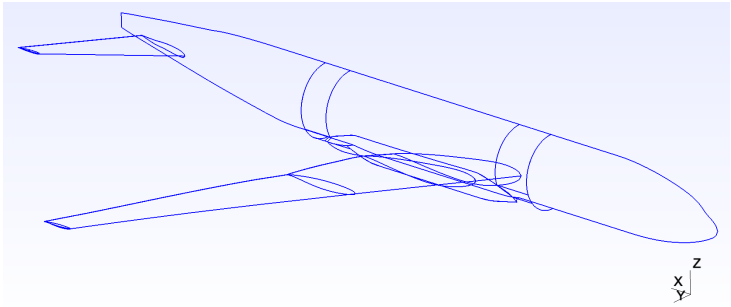

Figure 1: Geometry of the NASA Common Research Model (CRM).

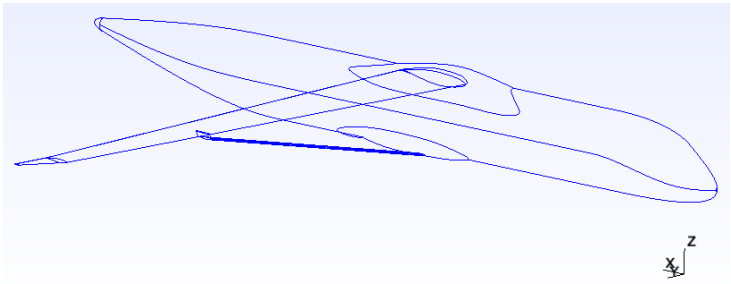

Figure 2: Geometry of the PADRI configuration (Platform for Aircraft Drag Reduction Innovation).

Table 1: Main geometrical parameters of targeted configurations.

Name	uCRM-9.0	uCRM-13.5	PADRI
Planform area $[m^2]$	383.74	384.05	161.00
Span [m]	58.76	72.00	55.6
MAC [m]	7.01	5.36	3.264
Aspect ratio	9.0	13.5	19.2
Taper ratio	0.275	0.250	0.256
1/4 Chord sweep [deg]	35.0	35.0	15.0
Dihedral [deg]	0.0	0.0	-4.0
Cruise Mach	0.85	0.85	0.72

3 METHODOLOGY

3.1 Aerostructural framework implementation

The aeroelastic analysis and optimization framework used in this study, developed by [5], is written in Python language and makes use of the OpenMDAO platform that is well suited for MDAO problems. This framework is able to solve both static and dynamic aeroelasticity problems. The way it works is presented in figure 3, each block (green boxes) corresponds to a specific component. The other boxes are used for linking the components together, feeding inputs from different outputs. Here two main disciplines run within the framework. First, the aerodynamic problem is solved either with DAFOAM or AVL depending on the chosen level of fidelity. Then, solving the structural problem is done by running MSC Natran finite-element analysis (FEA), either for a 1D beam model or a 3D wingbox model depending on the desired level of fidelity.

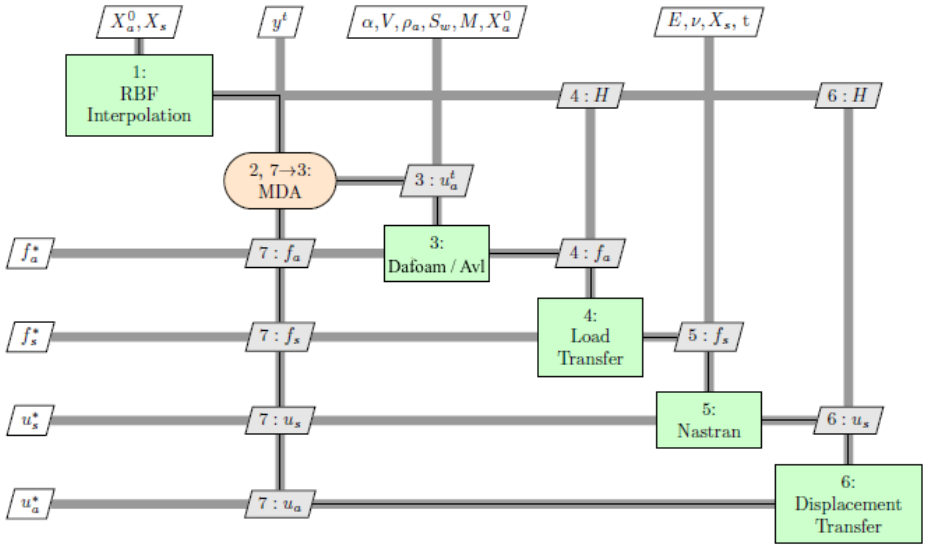

Figure 3: XDSM diagram of the static aeroelastic OpenMDAO HF/LF solver.

A mesh interpolation scheme that depends on the selected models is used for transferring loads from the aerodynamic solver to the structural mesh, and displacements from the structural solver to the aerodynamic mesh. In this work, low-fidelity computations are performed using both LF structural and aerodynamic models. Likewise, HF computations are carried out with both HF models.

The fluid-structure interaction problem is solved using an iterative partitioned approach. This process runs iteratively until convergence is achieved, based on selected quantities of interest.

3.2 Model description and generation workflow

For both high and low fidelity (HF and LF) simulations, only a half wing is considered, because a symmetry condition is applied in order to reduce computation time.

3.2.1 High-fidelity (HF) computations

In order to perform HF aerodynamic computations, the DAFOAM [10] solver is used to run CFD. For now, this aerodynamic code is used to solve steady Navier-Stokes equations. Airflow is considered viscous, turbulent and compressible. For generating the CFD mesh, the Pointwise meshing software is used based on the wing geometry in IGS format. The workflow to be followed in order to obtain HF aerodynamic loads is illustrated in figure 4.

The objective being to perform aerostructural analysis, the previously described aerodynamic solver needs to be coupled with a finite-elements analysis (FEA) solver, here the MSC Nastran software [11] is used. A three-dimensional wingbox finite-elements model (FEM) is generated as a BDF file. This wingbox shell-model breaks down into several components, upper and lower skin, ribs, spars and stiffeners. Skin, ribs and spars are represented using shell elements (CQUAD4), and stiffeners are represented using beam elements (CBAR). A Python module has been specifically developed to generate this model based on wing geometrical and material properties inputs. An example of a so

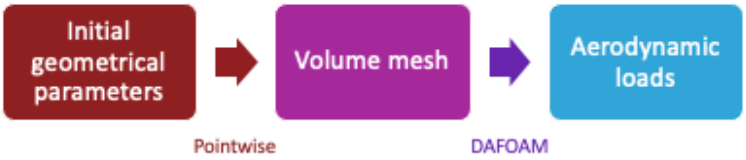

Figure 4: HF aerodynamic computational workflow.

developed FE mesh for the CRM wing is presented in figure 5.

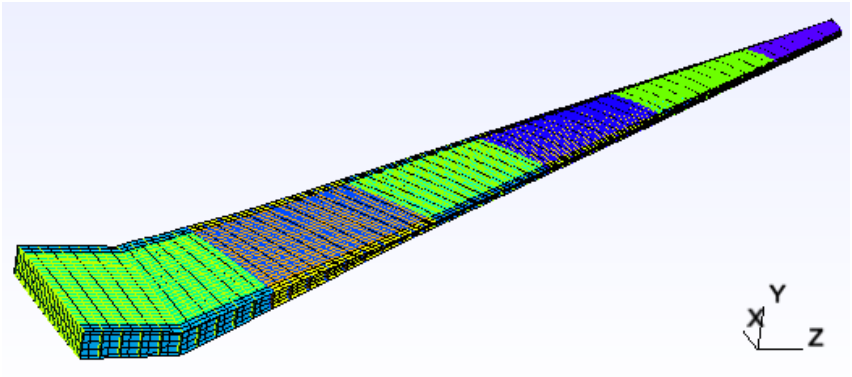

Figure 5: CRM structural FE model generated using dedicated module.

The wingbox structural models used in this work for uCRM-9.0 and uCRM-13.5 have been validated by comparing with results from [8]. Interpolation between aerodynamic and structural meshes is used to transfer loads and displacements. This is performed thanks to radial basis functions (RBF), using Thin Plate Splines (TPS) approximation developed in [12].

For now only linear FEA has been considered and tested, but the possibility to easily switch from a linear to a non-linear structural solver is also implemented for later use.

3.2.2 Low-fidelity (LF) computations

In order to perform LF aerodynamic computations, the AVL code [13] is used to carry out VLM (Vortex Lattice Method) computations, the corresponding model is generated through a dedicated Python module based on wing geometrical properties inputs. The model is defined through a certain number of control points, and associated chords, and twists. The workflow to be followed in order to obtain LF aerodynamic loads is presented in figure 6.

This VLM solver is also coupled to MSC Nastran [11]. Contrary to HF computations, a one-dimensional finite-elements model (FEM) is generated as a BDF file. The wing is split into a certain number of beam elements (CBAR). Another specific Python module has been developed to generate this model based on the wing geometrical and material properties.

The beam elements used in this model correspond to a rectangular beam section. Geometrical parameters, namely height, length, skin and spar thicknesses are the parameters,

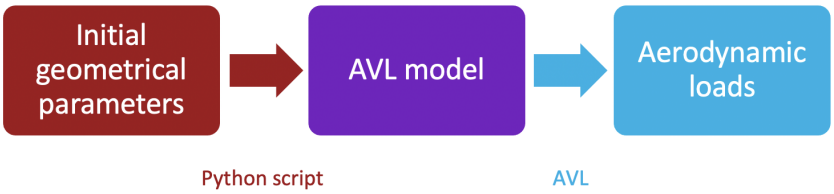

Figure 6: LF aerodynamic computational workflow.

are used as inputs, and corresponding stiffness properties are computed thanks to the script.

3.3 Optimizer and design variables

In this study, given the size of the problem, we have chosen to use a gradient-free optimizer. COBYLA optimizer is used for the rest of this work for both HF and LF optimizations. Relative tolerance of the optimizer is set to 10^{-3}.

The design variables considered in this study are the following: Structural thicknesses controled using B-splines (4 control points), Aspect ratio and Wing twist controled using B-splines (4 control points).

B-splines are used here in order to reduce the number of design variables. These are curves interpolated between a given number of control points which can then be used as design variables.

Initial values of the geometric design variables are set to the values of initial wing geometry. As for structural thicknesses, there are set to be decreasing linearly from 20mm to 2mm in the spanwise direction.

We describe here how modifications were applied to the CFD model, more specifically to the CFD mesh. The initial CFD mesh is deformed using FFD boxes rather than re-generated to avoid this time-consuming step. A FFD box is a box of control points that embeds the aircraft surface mesh. Any changes in FFD shape are then mapped onto the surface mesh.

Modifications of other models are not described as they are simply generated again as the process is fast and easy to automate.

4 APPLICATION CASES

The material considered in this study for structural models components is Aluminum alloy 7000 series. Its mechanical properties are presented in 2. Structural elements are sized to ensure that their maximum Von Mises stress is inferior to the material yield stress 2 with a safety factor of 1.5, corresponding to 280 MPa. Computations are considering both 1g and 2.5g load cases. The 2.5g extreme load case is the one being used for structural sizing. To be more specific, the 2.5g load case corresponds to the cruise condition where lift balances 2.5 times aircraft mass.

Our previous study [14] established that models developed are consistent with reference

Table 2: Material properties.

Parameter	Value
Density [kg/m3]	2780
Young's Modulus [MPa]	73100
Poisson Ratio	0.33
Yield Stress [MPa]	420

studies for uCRM-9.0 and uCRM-13.5 (see [8]).

4.1 Application to a HAR configuration

In this subsection, the optimization method described in section 3 is applied to the uCRM-13.5 high aspect ratio configuration to evaluate wing mass and examine how induced drag is affected when increasing aspect ratio. The optimization problem is described in table 3. Results are then compared to reference data for uCRM-9.0 from [14]. Structural and aerodynamic models are generated based on model chord and twist distributions, and wingpress geometry developed and presented in [8]. Flight conditions for each load case are described in table 4.

Table 3: Optimization problem applied to both application configurations (see subsection 3.3).

	Function/Variable	Bound	Comment
minimize	$\frac{CDi}{CDi_{ref}} + \frac{mass}{mass_{ref}}$		with $CDi_{ref} = 0.0250$ and $mass_{ref} = 15000.$
with respect to	Aspect ratio	$\leq$ 28.0	
	Wing twist [deg.]	$\geq$ -10.0, $\leq$ 10.0	B-spline parameters
	Skin thickness [mm]	$\geq$ 2.0	B-spline parameters
	Spar thickness [mm]	$\geq$ 2.0	B-spline parameters
subject to	Maximum stress at 2.5g	$\leq$ 280.0 MPa	Von Mises stress
	$CL_{1g} = 0.55$		
	$CL_{2.5g} = 0.55$*2.5		

Table 4: Flight conditions for each load case for MDO on uCRM-13.5 geometry.

Load case	1 g	2.5 g
CL (half-wing)	0.55	0.55*2.5
Mach number	0.85	0.85
Flight altitude [ft]	37,000	37,000

Results of HF and LF optimizations are summarized in table 5. As expected HF mass evaluation shows a 42.4% increase with regard to uCRM-9.0 reference case. Also, we observe a greater flexibility of the HAR configuration as wingtip displacement is 90.2%

Table 5: Results of HF and LF aeroelastic MDO for uCRM-13.5 geometry (uCRM-9.0 reference data from [8]).

Computation	High fidelity	Low fidelity
1g AoA [deg.]	2.49	1.68
Estimated cruise CDi [drag counts]	76.0	89.0
Baseline CDi (uCRM-9.0) [drag counts]	88.0	97.0
Deviation wrt baseline [%]	-13.6	-8.2
Optimized aspect ratio	14.9	15.5
Cruise wingtip displacement [m]	5.02	4.93
Baseline wingtip displacement (uCRM-9.0) [m]	2.64	2.85
Deviation wrt baseline [%]	90.2	73.0
Mass [kg]	15,952	13,865
Baseline mass (uCRM-9.0) [kg]	11,201	9,433
Deviation wrt baseline [%]	42.4	47.0
Number of iterations	11	6
Computation time [s]	17,237	1,548

higher than the one of uCRM-9.0. Finally, it appears that induced drag is reduced by 13.6% for the uCRM-13.5 configuration compared to the uCRM-9.0 reference configuration. Similar trends are observed when performing LF optimization. HF results shows a wing mass higher than LF results. It is to be noticed that LF optimization runs approximately 11 times faster than HF optimization.

4.2 Application to a HAR SBW configuration

Finally, we will evaluate mass reduction that can be be obtained when adding a strut to a HAR configuration, here the PADRI configuration. The optimization problem is described in table 3. For comparison purposes, we have designed a reference configuration where we have removed the strut from the original PADRI configuration. This geometry will be referred as PADRI-WS in the rest of the paper. The structure of the strut considered in this paper has a rectangular shape, with two parameters for each section, namely height (length is twice the height) and panel thickness. Flight conditions for each load case are described in 6.

Table 6: Flight conditions for each load case for MDO on PADRI SBW geometry.

Load case	1 g	2.5 g
CL (half-wing)	0.43	0.43*2.5
Mach number	0.72	0.72
Flight altitude [ft]	30,000	30,000

Results of HF and LF optimizations are summarized in table 7. Wingtip displacement is reduced by 32.9% with the HF computations. That is consistent with the strut reducing wing structure flexibility. It can also be observed that the HF mass is significantly reduced with regard to the PADRI-WS configuration. Indeed, the mass reduction is of 21.2%. This

Table 7: Results of HF and LF aeroelastic MDO for PADRI SBW geometry (PADRI-WS reference data).

Computation	High fidelity	Low fidelity
1g AoA [deg.]	1.32	0.94
Estimated cruise CDi [drag counts]	92.0	101.0
Baseline CDi (PADRI-WS) [drag counts]	89.0	97.0
Deviation wrt baseline [%]	3.4	4.1
Optimized aspect ratio	22.2	23.1
Cruise wingtip displacement [m]	1.06	1.43
Baseline wingtip displacement (PADRI-WS) [m]	1.58	1.95
Deviation wrt baseline [%]	-32.9	-26.7
Mass [kg]	9,878	9,102
Baseline mass (PADRI-WS) [kg]	12,541	11,982
Deviation wrt baseline [%]	-21.2	-24.0
Number of iterations	14	9
Computation time [s]	22,428	1,215

confirms the mass reduction potential of SBW configurations. Finally, induced drag is similar when compared to the PADRI-WS baseline configuration. Indeed, the deviation is below 5%. This is expected as the contribution of the strut to total lift is not significant. Similar trends are observed when performing LF optimization. HF results shows a wing mass higher than LF results. It is to be noticed that LF optimization runs approximately 18 times faster than HF optimization.

5 RESULTS

The comparisons with baseline values for both application cases are presented in figures 7, 8 and 9. Also, we have confirmed the expected result that induced drag is reduced when increasing the aspect ratio as displayed in figure 8. Finally, the performed optimizations have exemplified the mass reduction potential of a SBW configuration.

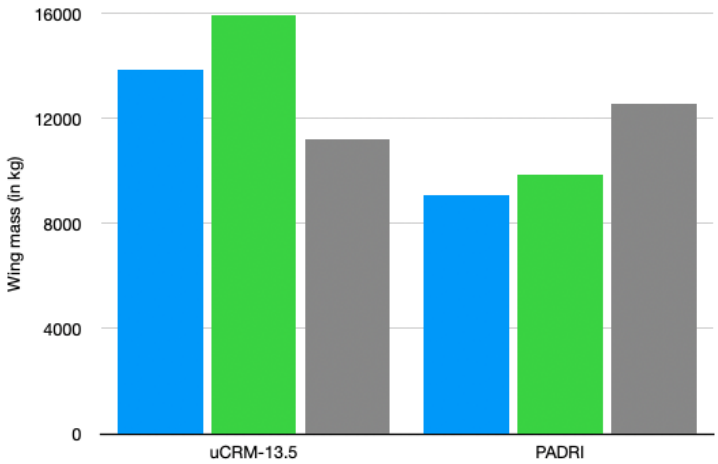

Figure 7: Synthesis of wing mass values for each configuration of interest (HF in green, LF in blue, HF baseline in grey).

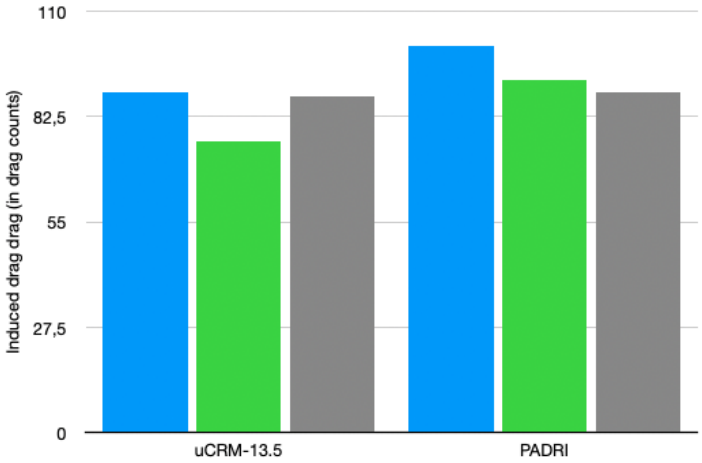

Figure 8: Synthesis of induced drag values for each configuration of interest (HF in green, LF in blue, HF baseline in grey).

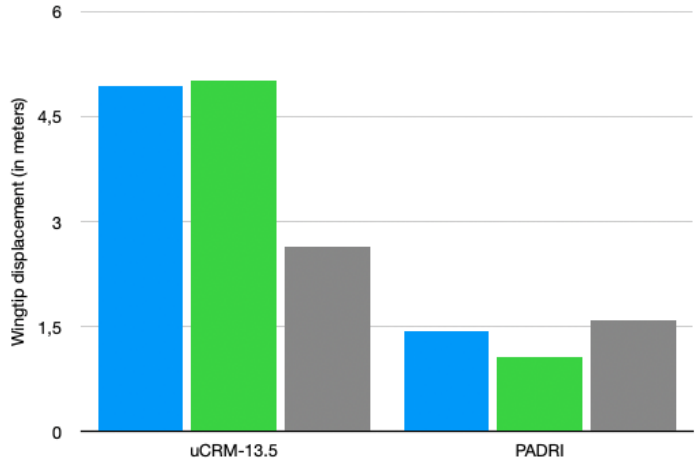

Figure 9: Synthesis of wingtip displacement values for each configuration of interest (HF in green, LF in blue, HF baseline in grey).

6 CONCLUSIONS

This work has demonstrated the aeroelastic optimization capabilities of our in-house framework applied to the HAR version of the NASA CRM, the uCRM-13.5 configuration as well as to the strut-braced PADRI configuration. This approach is effective for the two levels of fidelity mentioned in this paper.

In order to be able to evaluate the interest of a large number of configurations at preliminary design stage, it is necessary to make computation time more affordable. To this purpose, we are planning to use a multifidelity optimization approach that would allow us to mitigate computation costs. This is deemed to be a promising approach as the presented optimizations show that LF simulations run more than 10 times faster than HF simulations. The first step could be to use a strategy close to the one we described in [15], and later we would use MFEGO methodology as presented in [16].

AKNOWLEDGMENT

The work presented in this paper has been funded by the European Union in H2020-EU.3.4.5.10 through the CleanSky2 project U-HARWARD, under grant Grant agreement ID: 886552

REFERENCES

[1] T. Brooks, G. Kennedy, and J. Martins. High-fidelity multipoint aerostructural optimization of a high aspect ratio tow-steered composite wing. 01 2017. doi:10.2514/6.2017-1350.

[2] G. K. W. Kenway and J. R. R. A. Martins. Multipoint High-Fidelity Aerostructural Optimization of a Transport Aircraft Configuration. *Journal of Aircraft*, 51(1):144–160, Jan. 2014. doi:10.2514/1.C032150. URL `https://arc-aiaa-org.rev-doc.isae.fr/doi/10.2514/1.C032150`. Publisher: American Institute of Aeronautics and Astronautics.

[3] M. C. Kennedy and A. O'Hagan. Predicting the output from a complex computer code when fast approximations are available. *Biometrika*, 87(1):1–13, 2000. ISSN 00063444.

[4] D. R. Jones. A taxonomy of global optimization methods based on response surfaces. *Journal of Global Optimization*, 21(4):345–383, Dec 2001.

[5] J. Mas-Colomer. *Aeroelastic Similarity of a Flight Demonstrator via Multidisciplinary Optimization*. PhD thesis, 12 2018.

[6] J. M. Colomer. Aerostructure package, 2019. URL `https://github.com/mid2SUPAERO/aerostructures`.

[7] J. S. Gray, J. T. Hwang, J. R. R. A. Martins, K. T. Moore, and B. A. Naylor. Openmdao: an open-source framework for multidisciplinary design, analysis, and optimization. 2019.

[8] T. R. Brooks, G. K. Kenway, and J. R. R. A. Martins. Undeflected Common Research Model (uCRM): An Aerostructural Model for the Study of High Aspect Ratio

Transport Aircraft Wings. In *35th AIAA Applied Aerodynamics Conference*. American Institute of Aeronautics and Astronautics. doi:10.2514/6.2017-4456.

[9] NASA. Nasa common research model, 2017. URL `https://commonresearchmodel.larc.nasa.gov/`.

[10] P. He, C. Mader, J. Martins, and K. Maki. Dafoam: An open-source adjoint framework for multidisciplinary design optimization with openfoam. *AIAA Journal*, page 2019, 10 2019. doi:10.2514/1.j058853.

[11] R. S. Lahey, M. P. Miller, and M. Reymond. Msc/nastran reference manual, version 68. *The MacNeal-Schwendler Corporation*, 1994.

[12] T. C. S. Rendall and C. B. Allen. Unified fluid–structure interpolation and mesh motion using radial basis functions. *International Journal for Numerical Methods in Engineering*, 74(10):1519–1559, 2008. doi:https://doi.org/10.1002/nme.2219. URL `https://onlinelibrary.wiley.com/doi/abs/10.1002/nme.2219`.

[13] M. Drela and H. Youngren. Avl overview, 2013. URL `http://web.mit.edu/drela/Public/web/avl/`.

[14] E. B. Yoann Le Lamer, Joseph Morlier and P. He. Aeroelastic analysis of high aspect ratio and strut-braced wings. In *ICAS 2022*, Stockholm, Sweden, 2022. URL `https://www.icas.org/ICAS_ARCHIVE/ICAS2022/data/papers/ICAS2022_0560_paper.pdf`.

[15] Y. L. Lamer, G. Quaglia, E. Bénard, and J. Morlier. Multifidelity aeroelastic optimization applied to har wing. In *Aerobest 2021*, pages 454–472, Virtual event, PT, 2021. URL `https://oatao.univ-toulouse.fr/28740/`.

[16] N. Bartoli, M. Meliani, J. Morlier, T. Lefebvre, M.-A. Bouhlel, and J. Martins. *Multi-fidelity efficient global optimization: Methodology and application to airfoil shape design*. 2019. doi:10.2514/6.2019-3236. URL `https://arc.aiaa.org/doi/abs/10.2514/6.2019-3236`.